Fluctuations of the Red Blood Cell Membrane: Relation to Mechanical Properties and Lack of ATP Dependence

James Evans,*† Walter Gratzer,* Narla Mohandas,† Kim Parker,‡ and John Sleep*
*King's College London, Randall Division of Cell and Molecular Biophysics, Guy's Campus, London, United Kingdom;
†Red Cell Physiology Laboratory, New York Blood Center, New York, New York; and ‡Department of Bioengineering, Imperial College, London, United Kingdom

ABSTRACT We have analyzed the fluctuations of the red blood cell membrane in both the temporal (($\omega(s^{-1})$) and spatial ($q(m^{-1})$) frequency domains. The cells were examined over a range of osmolarities leading to cell volumes from 50% to 170% of that in the isotonic state. The fluctuations of the isotonic cell showed an $\sim q^{-3}$-dependence, indicative of a motion dominated by bending, with an inferred bending modulus of $\sim 9 \times 10^{-19}$J. When the cells were osmotically swollen to just below the point of lysis (166% of physiological volume), a q^{-1}-dependence of the fluctuations supervened, implying that the motion was now dominated by membrane tension; estimated as $\sim 1.3 \times 10^{-4}$ nm^{-1}. When, on the other hand, the cells were osmotically dehydrated, the fluctuation amplitude progressively decreased. This was caused by a rise in internal viscosity, as shown by measurements on resealed ghosts containing a reduced hemoglobin concentration, which displayed no such effect. We examined, in addition, cells depleted of ATP, before the onset of echinocytosis, and could observe no change in fluctuation amplitude. We conclude that the membrane fluctuations of the red cell are governed by bending modulus, membrane tension, and cytosolic viscosity, with little or no dependence on the presence or absence of ATP.

INTRODUCTION

The mechanical characteristics of red cell membranes are without parallel in any other known materials, combining an exceptional resistance to changes in area with a low, fluid-like shear response and bending resistance. These characteristics enable the normal red blood cell to undergo large distortions reversibly at constant volume under high shear stresses and to survive repeated passage through capillaries much narrower than its own principal dimension. Quantitative studies of membrane properties in vitro have in general been based on the application of large deformations, most often with the aid of the micropipette, and have delivered values for the shear, area, and bending moduli. (See Mohandas and Evans (1) for a review.)

The first recorded observations of an undulatory motion in the red cell membrane dates from the late 19th century, when Browicz (2) described the now familiar ''flicker'' phenomenon, readily seen in the light microscope. Its origin became a source of debate, but a study by Parpart and Hoffman (3) concluded that it is Brownian in character. The first quantitative analysis of red cell membrane fluctuations was undertaken by Brochard and Lennon (4,5), who used phase-contrast microscopy to extract a frequency spectrum and space correlation function from the thickness at two locations. They developed a model in which the cell is represented by two parallel flat membranes, excited thermally, from which they derived a value of the bending modulus, comparable to those determined later by methods involving the application of forced deformations (6,7).

A more refined model was developed by Helfrich and Servuss (8), and was tested by a variety of techniques by Sackmann and co-workers (9–15). Zilker et al. (9) monitored the upper membrane surface (in effect, the cell thickness) by interference reflection microscopy, and derived a bending modulus close to that of Brochard and Lennon. They also obtained a relation between the mean-square fluctuation amplitude, $\langle U_q^2 \rangle$, and the mode number, q, which, in the theory of Helfrich and Servuss, implied that the deformation is determined by bending modulus and not by tension. In another study from the same laboratory, Strey et al. (10) observed the movement of the cell rim at four equidistant points and derived the amplitudes of the first three fluctuation modes from the time autocorrelation function, and from the first of these (which they termed the hindered-translation mode) they extracted a lower value of the bending modulus than in the previous work. Most recently, Popescu et al. (16) measured the fluctuation across the cell of the separation between the upper and lower membrane surfaces using a new (''Hilbert phase'') microscopic technique, and reported a different outcome from that of Zilker et al. (9), namely a q^{-2}- dependence of the mean-square amplitude, which they took to imply a tension-dominated motion. The values for the bending modulus resulting from all the above fluctuation studies vary from 4×10^{-19} to 7.5×10^{-21} J.

A further aspect of red cell membrane fluctuation was introduced by Levin and Korenstein (17), and enlarged in a series of subsequent reports from the same laboratory ((18,19) and earlier references cited therein). They concluded from their observations on cells depleted of ATP that the membrane fluctuations are the result of an ATP-dependent process as much as of thermal agitation. They attributed the effect to

Submitted July 24, 2007, and accepted for publication January 2, 2008.

Address reprint requests to John Sleep, E-mail: john.sleep@kcl.ac.uk.

Editor: Petra Schwille.

0006-3495/08/05/4134/11 $2.00

doi: 10.1529/biophysj.107.117952

turnover of ATP on the short actin filaments that form the junctions of the membrane skeletal network (18).

We have used a simple microscopic technique, combined with a new computational method based on image processing, to characterize the red cell membrane fluctuation in terms of the motion at closely spaced points around the projected periphery of the cell. We have extended the measurements to the effects of volume changes and of ATP depletion. Whereas both increases and decreases in volume were accompanied by changes in fluctuation amplitude, we could detect no significant influence on fluctuations of ATP depletion. We also offer evidence that membrane tension largely governs the fluctuation in swollen, though not in native discoid cells, in which the existence of a small membrane tension is nevertheless compatible with our data.

MATERIALS AND METHODS

Sample preparation

Fresh red cells were obtained from healthy donors by centrifugation of fingertip blood, drawn into 10% citrate-dextrose solution (Sigma, St. Louis, MO). The cells were washed with phosphate-buffered isotonic saline (PBS), and suspended in PBS containing 1 mg ml^{-1} fatty-acid-free bovine serum albumin (Sigma). Osmolarities were adjusted as required by addition of sucrose or water, and the tonicity was checked with a freezing-point osmometer (Osmomat 030, Gonotec, Berlin, Germany).

For microscopy, a chamber was constructed by separating a coverslip, which had been cleaned by flaming, from its slide with streaks of petroleum jelly (Vaseline) at two opposite edges, and cementing the coverslip to the slide at its corners with Superglue (butylcyanoacrylate). In most experiments, the surfaces of the chamber were bare glass. Cells at 0.5% hematocrit in PBS containing 0.1% bovine serum albumin were applied to this chamber at an open end and allowed to enter by capillarity. The slide was then inverted and left to rest for 5 min to allow the cells to settle and adhere. Unattached cells were flushed out by perfusing the chamber several times with PBS (without albumin). The slide was then ready for observations. Three procedures were used to determine whether, and to what extent, membrane fluctuations were perturbed by adhesion to the substrate.

1. Coverslips were coated with poly-L-lysine by spreading with a solution of 20 $\mu g\ ml^{-1}$ poly-L-lysine (molecular weight 3000) (Sigma) in water, leaving this in place for 5 min, then rinsing with water and drying in a desiccator for several hours.
2. Instead of imaging cells attached to the underside of the coverslip, as described above, we allowed cells in the suspension to settle onto the bottom of the chamber. Instead of flushing out loose cells, all cells, however weakly attached, were left in place, and could then be examined.
3. Even when treated in this manner, the cells showed no translational drift, implying that some interaction with the glass persisted. We therefore looked for and found a surface to which there was no discernible attachment: a thin layer of low-melting agarose gel was applied to the slide by spreading a 1% solution of agarose (Sigma) in PBS on the warmed glass and allowing it to set. On this surface the cells drifted freely.

The instrumental baseline for a rigid body was established by measurements on fixed cells. These were prepared in situ by infusing glutaraldehyde in PBS into the observation chamber in four steps of increasing concentration up to 1% at intervals of ~1 min. After a further 10 min, excess reagent was flushed out with PBS.

For rapid depletion of ATP, cells were incubated at 37°C for 1 h in 150 mM NaCl, 10 mM HEPES, 6 mM iodoacetamide, 10 mM inosine, 1 mM EGTA, pH 7.4 (20). The ATP content was determined by the luciferin-luciferase assay, and found to be <1% of the original concentration. Most cells remained unchanged in shape for a period of at least 1 h, as demonstrated by Feo and Mohandas (21), after which echinocytosis set in.

Changes in tonicity of the suspending medium were made in situ. The mean cell volume at each tonicity was derived from the relation given by Lew and Bookchin (22), and the internal viscosity from the data of Cokelet and Meiselman (23). After each measurement at altered tonicity, the medium was again changed to isotonic, and the fluctuation was again measured to determine the extent of reversibility.

Cells with reduced hemoglobin content were prepared by lysis with two volumes of 10 mM sodium phosphate, 1 mM ATP, 1 mM $MgCl_2$, pH 7.4, on ice. This was followed by addition of 10× concentrated PBS containing Mg-ATP to restore isotonicity. The cells were then incubated at 37°C for 30 min to effect resealing, and washed with PBS. To check the mean cell hemoglobin concentration, a fixed volume of packed cells, measured in a hematocrit tube, was lysed and the hemoglobin concentration of the lysate was measured spectrophotometrically at 577 nm after centrifugation. Mean volumes of the hemoglobin-depleted cell populations were measured at each tonicity with a heamatocrit tube.

Microscopy and sample manipulation

Single cells were examined with a standard Zeiss microscope bolted to an antivibration table. Most studies were carried out under bright-field illumination with a 415-nm (2-nm bandpass) interference filter to monitor hemoglobin absorbance. A 100× Zeiss objective was used, with a numerical aperture set at 0.8, and a condenser aperture to correspond. Illumination was from a 100-W mercury arc. The images were recorded as 5-s videos (25 frames/s) with an Andor Luca camera, the image magnification corresponding to19 nm/pixel. The 14-bit stacked tif files were processed using MATLAB (The Mathworks, Natick, MA). The suspending medium could be repeatedly changed without disturbing the focus, with the aid of a filter-paper wick. Each medium change and the associated data measurement were completed in ~1 min. To avoid artifacts from photochemical damage it was necessary to minimize the exposure of the cells to the 415-nm light. The field-stop was therefore set so that only one cell at a time was illuminated. For reflection interference contrast (RIC) microscopy a Zeiss Antiflex Neofluor 63× oil-immersion lens was used with illumination by a 100-W mercury arc via a 546-nm interference filter. A polarizing beam-splitter was substituted for the dichroic mirror for epi-illumination

Analysis of cell edge movement

A method was developed, depicted schematically in Fig. 1 and described in the Appendix, of extracting the position of the cell edge, to give $U_{\theta,t}$, the excursion from the mean position, as a function of angular location around the circumference (θ) at 1° intervals, and of time (t) in steps of 0.04 s.

The time-average of $U^2_{\theta,t}$ gives the mean-square fluctuation as a function of angular position, $\langle U^2_\theta \rangle$, and by averaging this over all angles we gain the variance of fluctuation for the entire cell, $\langle U^2 \rangle$, and the root mean-square value, $\sqrt{\langle U^2 \rangle}$, which we will denote by $\overline{U}$. The Fourier transforms of $U_{\theta,t}$ in space and time give the mean-square amplitude as a function of wave number, $\langle U^2_q \rangle$, and frequency $\langle U^2_\omega \rangle$, respectively, as follows:

$$\langle U^2_q \rangle = \langle |\Im\{U_{\theta,t}\}_q|^2 \rangle_t; \quad (1)$$

$$\langle U^2_\omega \rangle = \langle |\Im\{U_{\theta,t}\}_\omega|^2 \rangle_\theta. \quad (2)$$

These parameters, derived from experimental measurements, can be related to properties of the cell membrane by way of the available theoretical models. The fluctuation amplitude for each mode, $q = 1,2,3\ldots$, in wavelengths/cell, is measured. In practice, it proved useful to divide the mean-square amplitude into its low $\langle U^2_q \rangle_{low}$ ($q \le 10$ $cell^{-1}$) and high $\langle U^2_q \rangle_{high}$ ($q > 10$ $cell^{-1}$) components. The mean-square fluctuation in the time domain was similarly divided into two components, $\langle U^2_\omega \rangle_{low}$ ($\omega \le 2$ s^{-1}) and $\langle U^2_\omega \rangle_{high}$ ($\omega > 2$ s^{-1}).

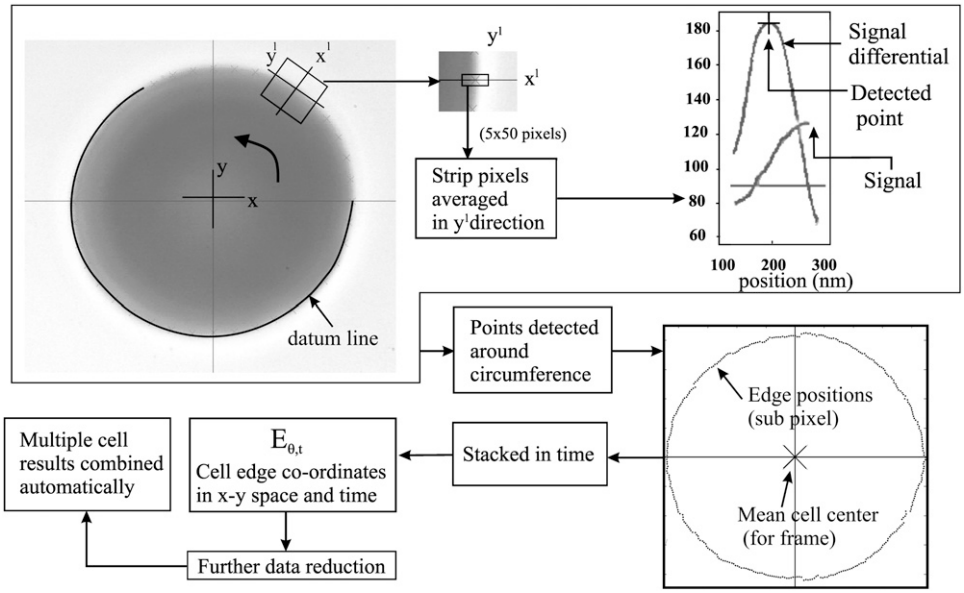

FIGURE 1 Membrane edge location procedure. An initial spline giving the approximate edge of the cell is obtained by a simple thresholding method (*datum line*). Using this as a starting point, strips perpendicular to the cell edge are generated for each video frame around the entire periphery at 1° intervals. These are then used to locate the edge position with the aid of a subpixel algorithm. The process is repeated for each video image, and results for multiple videos are combined to generate statistically meaningful results.

The choice of these limits is dictated by the abrupt change of slope in the power spectra when plotted on a linear scale.

As previously observed (4), $\langle U_\omega^2 \rangle$ conforms to a power-law dependence, such that $\langle U_\omega^2 \rangle \propto \omega^{-\gamma}$, and the value of γ was determined for each experiment, using a least-squares fit. Similarly, we observed an approximate power-law relationship of the form $\langle U_q^2 \rangle \propto q^{-\mu}$, for q between 6 and 20 cell^{-1}, and the value of μ was also determined using the method of least squares.

The theoretical treatment by Pécréaux et al. (24,25), deriving from the analysis of Helfrich and Servuss (8), relates the mean-square amplitude and the mode (q) to membrane tension (σ) and bending modulus (κ) as follows:

$$\langle |U_q|^2 \rangle = \frac{k_B T}{2\sigma}\left[\frac{1}{q} - \frac{1}{\sqrt{\sigma/\kappa + q^2}}\right]. \quad (3)$$

Two limiting cases, in which fluctuation behavior is dominated by membrane tension and by bending modulus, respectively, are described by the equations

$$\langle |U_q|^2 \rangle = \frac{k_B T}{2\sigma q^\mu} \quad (\mu = 1) \quad (4)$$

(for $\sigma \gg \kappa$), and

$$\langle |U_q|^2 \rangle = \frac{k_B T}{4\kappa q^\mu} \quad (\mu = 3), \quad (5)$$

(for $\sigma \ll \kappa$), where k_B is the Boltzmann constant and T the temperature. The value of the measured exponent, μ, will then indicate whether the fluctuations are dominated by bending modulus ($\mu \approx 3$, predicted for $\sigma \ll \kappa$) or by membrane tension ($\mu \approx 1$, predicted for $\sigma \gg \kappa$). Under such limiting conditions, Eqs. 4 and 5 will deliver the value of σ or of κ. To validate this procedure, we applied it to video images of stearoyloleoyl phosphatidylcholine giant vesicles (data kindly provided by Dr. P. Cicuta), and found that the derived values agree with the published data.

A relationship for calculating the bending modulus from the first fluctuation mode has also been derived by Strey et al. (10) from the model of Peterson et al. (15), namely:

$$\kappa = \frac{(6 \times 10^{-3}) k_B T R^2}{\langle U_{q=1}^2 \rangle}, \quad (6)$$

where R is the cell radius. We have also used this equation to calculate bending moduli for comparison with results from Eqs. 3 and 5.

RESULTS

Cell shape

Examples of shapes of cells in different osmotic conditions, viewed by RIC and filtered bright-field imaging, are shown in Fig. 2. The RIC image of the isotonic cell (Fig. 2 *e*) shows a dark ring of contact with the substrate, with an indentation in the center consistent with a biconcave shape. The same applies to the corresponding filtered bright-field image (Fig. 2 *b*), which reflects the thickness profile. The biconcave shape was confirmed by focusing through the occasional cell hanging by its edge from the coverslip. The images of a dehydrated cell (Fig. 2, *a* and *d*) show a thicker ring of contact with the coverslip and a deeper concavity. The images of the swollen cell (Fig. 2, *c* and *f*) imply a spherical or oblate spheroidal form with a small circular central contact area.

Single-cell measurements

Fig. 3 *a* shows the mean-square amplitudes of the first 11 modes, $\langle U_q^2 \rangle_{low}$, of a single cell, together with a representation of the form of the first four. Fig. 3 *b* shows the autocorrelation function for a cell before and after subtraction of the centroid movement, designated by Strey et al. (10) as the first, or ''hindered translation'', mode, which corresponds to the translation of the cell about its attachment zone. When this is eliminated, the next mode ($q = 2$) becomes the most prominent. Cells fixed with glutaraldehyde showed a total fluctuation, $\overline{U}$, of the cell with a standard deviation of ~4 nm, compared to 23 nm for an unfixed cell.

Fig. 4 shows, again for a single cell, how the space (*a*) and time (*b*) power spectra of the fluctuation change when the cell

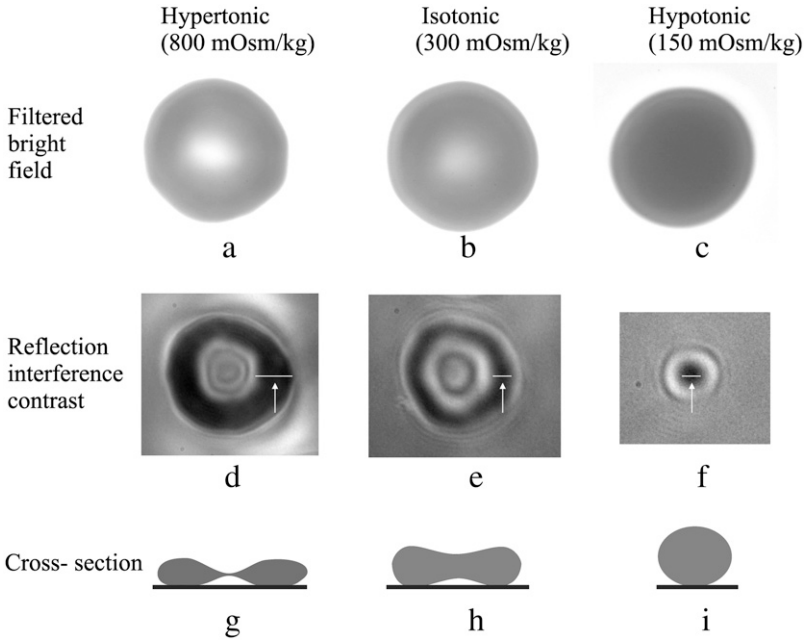

FIGURE 2 Images of cells in differing osmotic conditions. (*a* and *d*) Cells under hypertonic conditions in bright-field (hemoglobin Soret-band filter) and reflection interference contrast. (*b* and *e*) Equivalent images of cells under isotonic conditions. (*c* and *f*) Equivalent images for hypotonic cells. For the RIC images, due to the π phase shift at the interface, the contact region is dark and can be readily distinguished from the other dark bands, since these show clear thermal fluctuations. Arrows indicate the contact regions for the three conditions, and it can be seen that in the hypotonic state this is restricted to the center of the cell. The spacing of the other rings is closest in the hypertonic condition, representing the relatively steep angle of the membrane where it nears the central dimple. Images in the top row, which represent hemoglobin absorption, are consistent with these qualitative observations. The schematic diagrams (*g–i*) are the corresponding inferred cross sections.

undergoes a transition from the native (isotonic), discoid state to a highly hypotonic swollen form, induced by reducing the osmolality of the medium from 300 to 150 mOsm kg^{-1}. Results for a glutaraldehyde-fixed cell are included to show the limits of precision. It can be seen (Fig. 4 *a*) that the slope, μ, of the linear portion of the plot of mean-square amplitude, $\langle U_q^2 \rangle$, against mode number, q, undergoes a large change from ~3 in the isotonic to ~1 in the hypotonic, swollen state. These correspond in the formulation of Pécréaux et al. (24) (Eqs. 3 and 4) to the theoretical values for deformations dominated by bending modulus and tension, respectively. From the intercepts, values of the bending modulus and tension can be derived. The slopes, γ, of the linear time power-spectrum plots (Fig. 4 *b*) are ~0.9 for the isotonic and ~0.3 for the hypotonic state.

Effects of adhesion to the substrate

To determine whether the observed fluctuations were significantly perturbed by adhesive interactions with the substrate, cells were examined in four different states of attachment, with measurements from~90 cells in each instance. 1), Cells were allowed to attach to the glass coverslip directly, and unattached cells were flushed away with buffer; 2), cells were applied to a coverslip coated with low-molecular-weight polylysine; 3), cells were allowed to settle on the bottom of the viewing chamber without flushing and were observed in that position, thus affording a mixed population of attached cells and unattached or lightly attached cells, which would have been removed by flushing with buffer; and 4), cells were observed after deposition on an agarose-coated slide at the

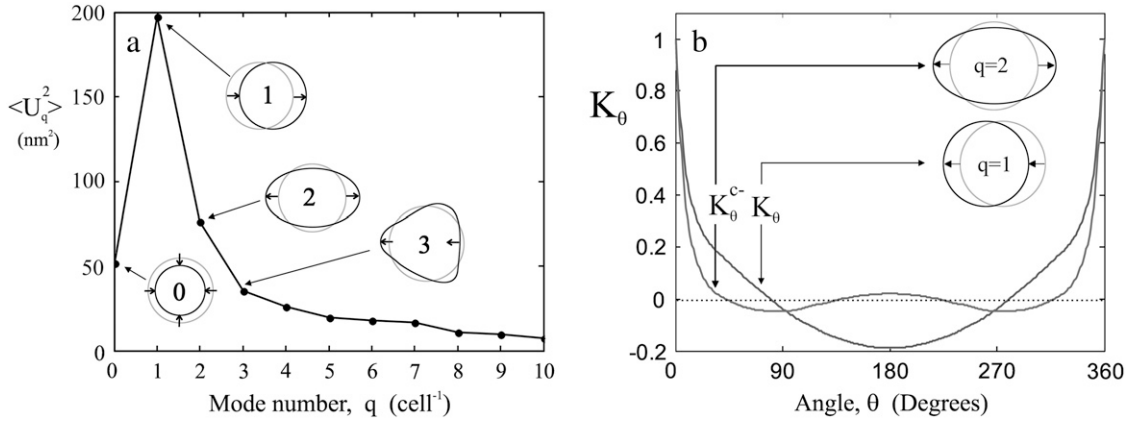

FIGURE 3 Modal decomposition of cell edge movement. (*a*) Contributions of successive modes (squares of amplitudes) to the spatial power spectrum, P_ϕ, of the edge fluctuation for the first 11 modes (schematic representations are shown for the first four modes). (*b*) Autocorrelation functions of membrane fluctuations measured before, K_θ, and after, K_θ^{c-}, subtraction of the centroid movement, with schematic insets showing the dominant mode in each case.

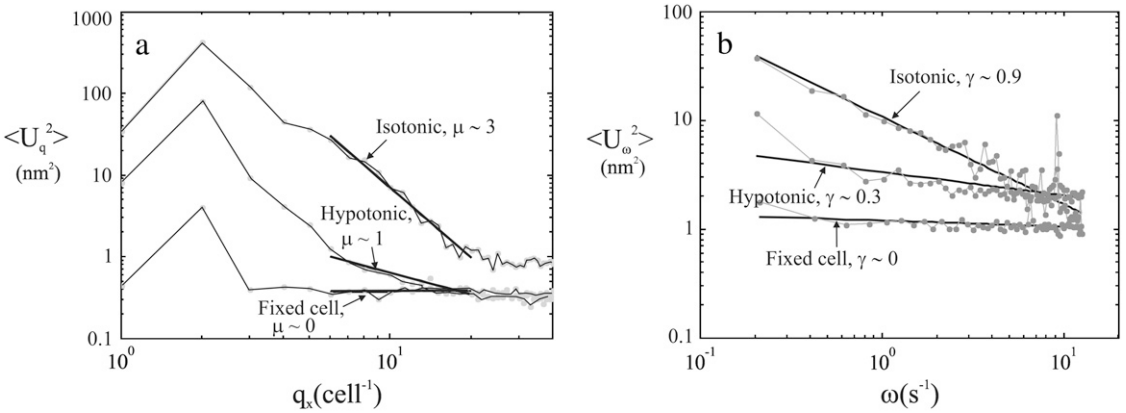

FIGURE 4 Space and time power spectra for a typical single cell in isotonic and hypotonic conditions. (*a*) The space power spectrum displays a power-law relationship in the midregion ($6 < q < 20$ cell^{-1}) giving 2.85 and 0.87 for the exponent, μ, in isotonic and hypotonic conditions, respectively. Mean values for different cells are close to 3 and 1, respectively. (*b*) The time power spectrum follows a power-law relationship, with exponents, γ, of 0.91 and 0.28 in the isotonic and hypotonic states.

bottom of the viewing chamber. On this highly hydrophilic, uncharged surface the cells diffused slowly and continuously, giving no indication of any adhesive interaction. Fluctuation data for cells in these four conditions are set out in Table 1, from which it can be seen that there is little difference between any of them, and indicating that adhesive effects are negligible under all these conditions.

Effects of cell shape and volume

The following results refer in each case to an average over 15 cells, each cell having been separately subjected to the same range of osmotic conditions. To examine the effect of cell volume on membrane fluctuations, we varied the osmolality of the suspending medium on either side of physiological (300 mOsm kg^{-1}) from 154 to 1085 mOsm kg^{-1}. The cell volume and intracellular viscosity were derived from standard data (22,23). The calculated mean cell volumes at the limiting tonicities were 166% and 53% of physiological. The projected cell diameter changed monotonically with cell volume over the entire range. Fig. 5 shows the dependence of the projected diameter on osmolality. Between successive changes in medium the cells were brought back to the isotonic state to establish the extent of reversibility of the effects of each volume change.

TABLE 1 Fluctuation parameters for normal cells on four different surfaces

	A $n = 94$	B $n = 90$	C $n = 90$	D $n = 90$
$\sqrt{\langle U^2 \rangle}$ nm	23.6 ± 0.6	22.5 ± 0.8	23.8 ± 0.8	24.0 ± 0.7
$K_c \times 10^{-19}$ J (using Eq 5)	8.7 ± 0.3	9.1 ± 0.4	8.6 ± 0.4	8.1 ± 0.4

Cell groupings were (*A*) on untreated glass surface; (*B*) on polylysine-coated glass; (*C*) resting on untreated glass at the bottom of the observation chamber; and (*D*) on an agarose-coated surface. All values are mean ± SE.

We have decomposed the fluctuation amplitude into its constituent modes. Fig. 6 *a* indicates how the first four of these vary with the volume of the native cell. All four curves show a well-defined maximum at a volume slightly below that of the unperturbed cell. For mode 1, the maximum is at ~85% of the native volume, shifting slightly to lower volumes with increasing mode number. On the low-volume side of its maximum, the fluctuation amplitude drops steeply to a very low level

To examine further the nature of the fluctuation, we separated the signal into its low- and high-mode components, defining these as $q \leq 10$ and $q > 10$ cell^{-1}. As Fig. 6 *a* shows, the low-mode-number component has a much greater dependence on cell volume, with a fourfold variation over the volume range, and a well defined maximum at ~80% of the native volume. The high-mode-number component, by contrast, displays a relatively flat response. Fig. 7 *b* depicts the temporal counterparts of the spatial fluctuations shown in Fig. 7 *a*. Here, again, the low-frequency (taken as $\omega \leq 2$ s^{-1}) and high-frequency ($\omega > 2$ s^{-1}) components differ markedly in their volume response. The low-frequency component exhibits, as before, a strong volume dependence, with a well defined maximum at ~80% of native volume, whereas the high-frequency component varies little, especially between 80% and 120%. The total measured temporal fluctuation profile, from which the high- and low-frequency components are derived, is also shown (Fig. 6 *a*) . At volumes below that of the native state, the low-frequency fluctuations appear most prominent, whereas at higher volumes the high-frequency contribution predominates.

We have taken the power-law relationships between fluctuation amplitude and mode from the linear segments of plots shown in Fig. 4 (i.e., modes 6–20 cell^{-1}), averaging data for 15 cells throughout the volume range (discarding the segments at the high- and low-mode number extremes (24)). Fig. 8 *a* shows the volume dependence of the exponents γ and μ in

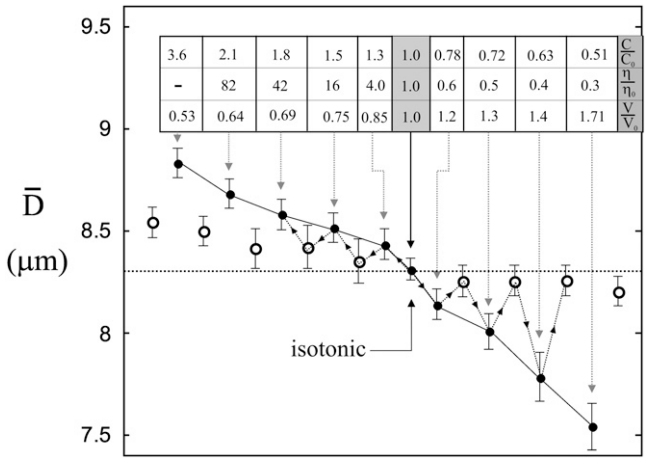

FIGURE 5 Relation between projected cell diameter and medium tonicity. Measured diameters, averaged over 15 cells, are shown as a function of medium osmolality. Tonicity was altered in successive steps (●), and brought back to isotonic and reanalyzed (○) between changes. Cells were measured first in the hypotonic and then in the hypertonic range in the sequence indicated by arrowheads joining the points. The osmolality, C, and the corresponding volume, V, relative to that in the isotonic state (22), and cytosolic viscosity, η (23), at each tonicity are tabulated, expressed relative to the values C_0 (300 mOsm kg^{-1}), V_0 (unity), and η_0 (10 cP) in the isotonic state. Note the sharp rise in viscosity at the highest tonicities.

the time and space power spectra. It can be seen that μ varies between ~2.6 and 3 over the volume range 80–140% of that of the unperturbed, isotonic cell, but falls sharply on further swelling, to ~1. In cells dehydrated to a volume <80% of normal, μ exhibits an abrupt fall to <0.5. The time power-spectrum exponent, γ, also shows a strong volume dependence, falling linearly from a maximum of 1.2 at a volume of 70% to ~0.2 in the maximally swollen cell, and more sharply to about the same level when the cells are dehydrated.

Fig. 8 *b* shows the bending moduli calculated by two methods, that of Strey et al. (10), based on the mode-1 fluctuation amplitude (Eq. 6), and that of Pécréaux et al. (24) (Eq. 5), which is only applicable to the data between 80% and 140% of native volume. This second method gives a value for κ of $8.7 \pm 0.3 \times 10^{-19}$ J (mean ± SE, $n = 30$) for the cell in the native state, whereas the first yields a value some three times greater. The theory of Pécréaux et al. (24) (Eq. 4) allows us also to calculate a value of $1.3 \pm 0.3 \times 10^{-4}$ Nm^{-1} (mean ± SE, $n = 15$) for the membrane tension, σ, in the swollen state (166% of native volume). The value of μ for the isotonic state appears to be just <3 (i.e., 2.8 ± 0.2), suggesting that there may be some tension-induced suppression of the fluctuations.

Hemoglobin-depleted cells

To determine whether and to what extent the fluctuation is regulated by internal viscosity, we performed measurements on cells containing 30% of the physiological hemoglobin concentration, with an internal viscosity therefore some 10 times lower than for intact normal cells in isotonic conditions (23). The metabolic state of these cells (resealed ghosts), as measured by the cytosolic Mg-ATP concentration, was similar to that of native cells, and so, also, as expected, was their shape. We found the resealed cells to be somewhat variable in volume, so that the tonicity required to generate a highly swollen population could not be precisely defined. We therefore restricted the maximum hypotonic volume increase to a nominal 130% of native (Fig. 6 *b*). By marked contrast with native cells, hypertonic volume reduction was not accompanied by any perceptible drop in membrane fluctuation amplitude. We conclude that the suppression of fluctuations in the intact cell under strongly hypertonic conditions is the result of the steep rise in hemoglobin concentration at elevated concentration (23).

When the cells with reduced hemoglobin content were swollen, they did not show the drop in fluctuation amplitude seen in the native cells (Fig. 6 *b*). The reason for this is not

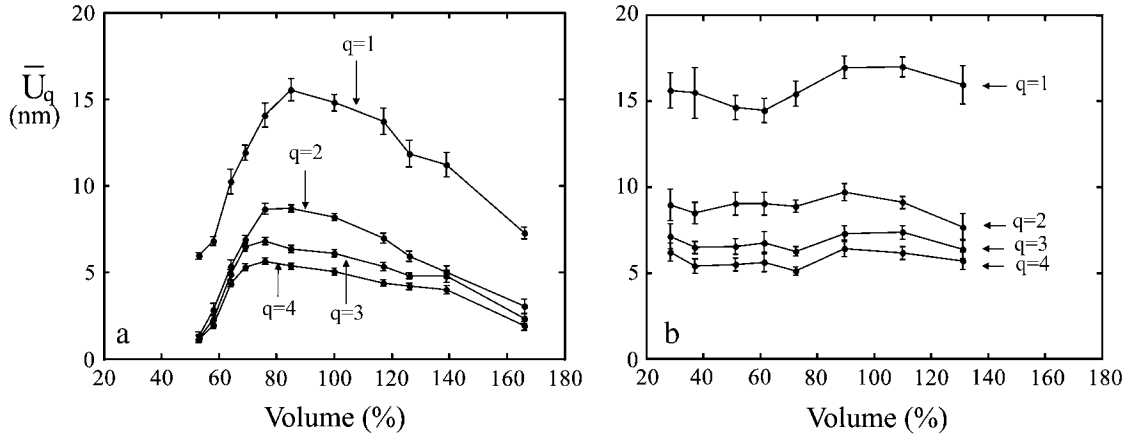

FIGURE 6 Effect of reduced hemogloblin concentration on fluctuations. Fluctuation amplitudes are shown for the first four modes of an intact cell (*a*) and for cells (resealed ghosts) containing ~⅓ of the normal hemoglobin concentration (*b*) for different cell volumes.

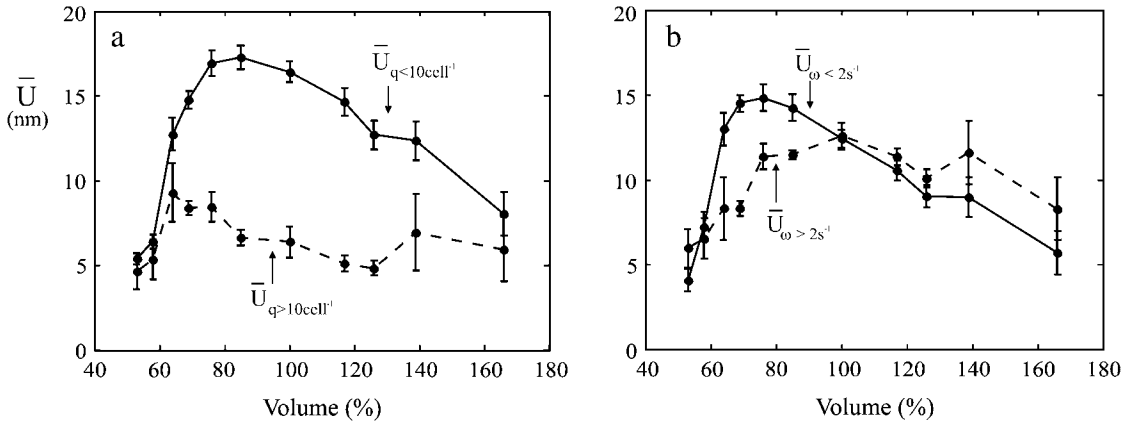

FIGURE 7 Decomposition of fluctuations into space and time components for different cell volumes. (*a*) Fluctuation amplitudes of low- and high-mode-number components ($q \leq 10$ cell^{-1} and $q > 10$ cell^{-1}, respectively). (*b*) Low- and high-frequency fluctuation amplitudes ($\omega < 2$ s^{-1} and $\omega > 2$ s^{-1}, respectively).

entirely clear but is probably due to the restricted volume increase (30%) that could be imposed on these cells without extensive lysis; in the native cells, the hypotonically induced changes of fluctuation amplitude predominantly occurred in the range that we were unable to explore in the resealed ghosts (close to the maximum volume of 166% of physiological).

Metabolically depleted cells: effect of ATP

The effect of ATP depletion on membrane fluctuation was measured on 90 cells before and after rapid metabolic depletion (20,21). Only cells that had undergone no shape change were studied in the depleted state. The results are set out in Table 2. The measured fluctuation amplitude and resolved components are tabulated, as well as the calculated bending modulus. Within the limits of experimental error, there was no difference between the properties of the fresh and the ATP-depleted cells.

DISCUSSION

The series of experiments carried out to determine the effect of cell adhesion on membrane fluctuation revealed no significant difference between cells on a bare glass surface, on lightly polylysine-coated glass, or on an agarose surface. Cells on agarose-coated glass could be seen to diffuse in the surface plane, and were therefore taken to interact negligibly with the surface. We could thus exclude artifacts resulting from adhesion to the substrate in any of the experimental conditions. It is noteworthy that even the coating of polylysine, at least of low molecular weight, and when deposited from a dilute (20 μg ml^{-1}) solution, as in our procedure, did not perturb the fluctuations. Such conditions have been used by previous workers for attaching cells to a glass surface (9–15,18). It is to be expected, however, that higher concentrations of polylysine, such as those shown by Hategan et al. (26) to lead eventually to lysis, would have profound affects on the fluctuation.

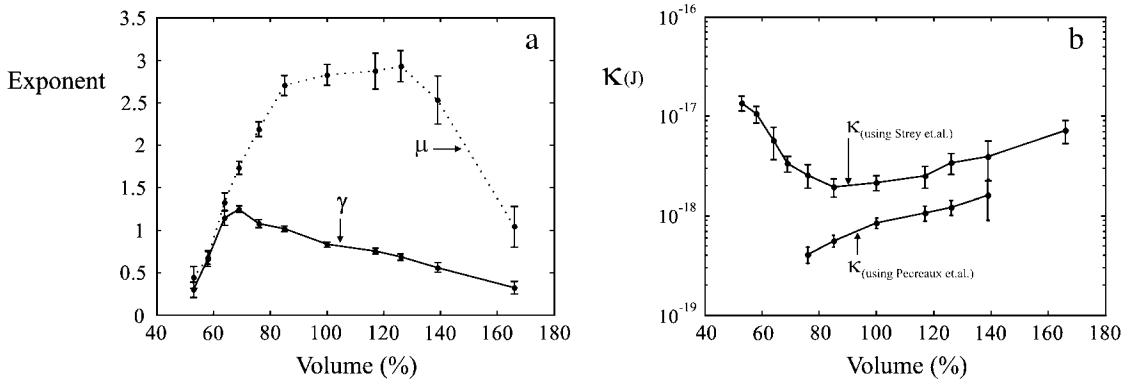

FIGURE 8 Dependence of the power-law exponents of the time and space power spectra on cell volume, and the derived values of membrane bending stiffness. (*a*) Exponents of the power-law relations of the time power spectrum (γ) and the space power spectrum (μ) as a function of cell volume. (*b*) Bending stiffness, κ, calculated by the methods of Strey et al. (10)) and Pécréaux et al. (24). (See text for explanation.)

TABLE 2 Membrane fluctuation parameters for normal and ATP-depleted cells

	Normal cells $n = 94$	ATP-depleted $n = 92$
$\sqrt{\langle U^2 \rangle}$ nm	23.6 ± 0.6	22.8 ± 1.0
$\sqrt{\langle U^2_{q\leq 10} \rangle}$ nm	20.1 ± 0.3	20.3 ± 0.9
$\sqrt{\langle U^2_{q>10} \rangle}$ nm	11.9 ± 0.6	10.5 ± 0.5
$\sqrt{\langle U^2_{\omega<2} \rangle}$ nm	14.2 ± 0.3	14.6 ± 0.8
$\sqrt{\langle U^2_{\omega>2} \rangle}$ nm	13.7 ± 0.6	14.3 ± 0.5
$K_c \times 10^{-19}$ J (using Eq 5)	8.7 ± 0.3	9.0 ± 0.3
$K_c \times 10^{-19}$ J (using Eq. 6)	25.0 ± 1.7	21.5 ± 1.2

All values are mean ± SE.

The projected diameter of a cell under observation (reflecting the degree of swelling and consequently of contact with the surface) changes monotonically with osmolality of the medium (Fig. 5). Fig. 5 also shows the almost complete reversibility of the projected diameter changes on return to isotonicity after each change of medium. There was, however, a systematic change in isotonic diameter after exposure of the cells to highly osmotically stressed conditions, especially in the hypertonic state in which the areas of adhesion are greatest (Fig. 2). It seems likely that this hysteresis does not reflect irreversibility of any adhesive interaction, which appears to relax in ~1 min, but rather slow recovery of the cell shape after separation of the membrane from the substrate.

The root mean-square fluctuation amplitude at the cell rim, $\overline{U}$, measured in this study on all surfaces, is ~23 nm, slightly lower, therefore, than the ~30 nm reported by Strey et al. (10), using a related method. We have found that at lower image contrast the measured amplitude tends to increase uniformly over the whole frequency range, and that, if measurements extend over longer periods (>1 min), the result is often affected by the tendency of the cell to drift slightly. The ensuing increase in apparent amplitude can be eliminated, as we have found, by subtracting the centroid movement. These considerations suggest that errors arising from limitations of image quality and from cell translation tend to increase, rather than decrease, the measured amplitude.

We have shown that cells partially depleted of hemoglobin (Fig. 6 *b*) have larger fluctuation amplitudes than the parent cell, but, more importantly, that the amplitude no longer displayed a steep fall with decreasing volume. This implies that the drop seen in normal cells results from the increase in hemoglobin concentration, and hence of cytosolic viscosity. With a 50% decrease in volume, the hemoglobin viscosity rises by ~100-fold (see data tabulated in Fig. 5). An alternative, or additional, explanation that cannot be excluded is that the hemoglobin at the high concentration binds to and rigidifies the membrane. Although oxyhemoglobin binds only very weakly to the membrane (27), or more particularly to its integral proteins, the interaction could become more significant at the higher hemoglobin concentration, probably at or near the solubility limit, in the dehydrated cells. The difference in fluctuations between normal and hemoglobin-depleted cells is much less at higher cell volumes, where the change in hemoglobin viscosity is small.

We have found, in agreement with earlier work, that the mean-square amplitude of the time power spectrum, $\langle U^2_\omega \rangle$, is proportional to $\omega^{-\gamma}$ over the full range of measured frequencies. Our observed value of γ of ~0.9 for the cells in isotonic medium changes markedly with cell volume, reaching a maximum of ~1.2 at 70% of native volume, and falling to a minimum of ~0.3 at 166%. Swelling causes a reduction in γ as higher-frequency components become more dominant (Fig. 8 *b*). For the spatial power spectrum, which adheres to a power-law relation, i.e., $\langle U^2_q \rangle \propto q^{-\mu}$, over the volume range 80–140% of native, we obtain a mean value for the exponent, μ of 2.6–2.9 (see Fig. 8). It would follow that the fluctuations are overwhelmingly controlled by the bending modulus throughout the range. Eq. 5 delivers a bending modulus, $\kappa = 3\text{–}12 \times 10^{-19}$ J over the range and a value of $\kappa = 9 \pm 0.3 \times 10^{-19}$ J for the isotonic condition. Estimation of membrane tension or bending modulus from the experimental measurements of mean-square fluctuation amplitude is straightforward in these limiting conditions of $\mu = 1$ and $\mu = 3$ (Eqs. 4 and 5, respectively). For intermediate values of μ, one should in principle be able to estimate both σ and κ from Eq. 3 by a multiparameter fit to the data, but the fits are poorly constrained and not reliable. To estimate an upper limit for the tension in the isotonic condition, we have taken the bending modulus calculated from Eq. 5 (since μ is close to 3), introduced this into Eq. 3, and then varied the membrane tension until the slope of the linear fit to Eq. 5 (within the relevant range of $q = 6\text{–}20$ cell^{-1}) started to drop below 3. The resulting upper limit for the membrane tension is $\sim 5 \times 10^{-7}$ Nm^{-1}. At the highest volumes, close to the point of lysis, we find that $\mu \approx 1$, which is consistent with Eq. 3 for $\sigma \gg \kappa$. In this limit, Eq. 5 can be used to estimate the membrane tension, σ, as $\sim 1.3 \pm 0.3 \times 10^{-4}$ Nm^{-1}, which is two orders of magnitude greater than our estimate of the tension in the isotonic cell (see below).

Popescu et al. (16) have applied a nonlinear fit based on the cytoskeleton confinement model of Gov et al. (28) to the relation between mean-square amplitude and mode number to extract values for bending modulus and membrane tension of $0.75 \pm 0.15 \times 10^{-20}$ J and $1.5 \pm 0.2 \times 10^{-6}$ Nm^{-1}. Our calculated value of tension in the membrane of the isotonic cell is of the same order as that inferred by Popescu et al., but our prediction of bending modulus is ~1 order of magnitude higher.

The existence of a tension in the red cell membrane was suggested by the authors of the first study of the red cell membrane by the micropipette technique (29), who found evidence for a small excess pressure (~23 Pa) in the cell, giving, by Laplace's theorem for an oblate ellipsoid, a tension of 1.2×10^{-5} Nm^{-1}. This pressure difference was later challenged as being too high by not less than an order of magnitude (30). Our conclusion that fluctuation is dominated

by bending modulus over a broad range of tonicities on either side of isotonic accords with that of Zilker et al. (9), but conflicts with Popescu et al. (16). The explanation may lie in a difference in experimental methods and/or the theoretical treatments used.

Membrane tensions as high as our value of $1.3 \pm 0.3 \times 10^{-4}$ Nm^{-1} for the red cell in the swollen state (166% of native volume) have been reported in nucleated cells (31,32) stressed by membrane-linked filaments, and the effects of increased tensions induced by different methods in isotonic red cell membranes have also been studied (26,33,34). Hategan et al. (26) give an experimental curve of time to lysis as a function of induced tension in the red cell, which suggests that tension at the level we have estimated, sustained for ~1 h should cause lysis of the cell. We did not attempt to verify this in a systematic way, but noted that when cells were left in this state for periods of over half an hour, some lysis had occurred.

As Fig. 7 shows, decomposition of the fluctuations in time and space reveals that low modes ($q < 10$ $cell^{-1}$) and low frequencies ($\omega < 2$ s^{-1}) dominate the fluctuations and these modes are most strongly affected by changes in volume. They are suppressed in the swollen cell, but increase when the cell volume undergoes a modest reduction (to ~80% of the normal volume). A likely explanation of this rise in fluctuation amplitude is a small decrease in membrane tension accompanying the volume change, which renders the structure more flaccid. On further volume reduction, beyond ~80% of physiological, the effects of hemoglobin concentration are likely to override any changes in membrane tension.

Our quantitative interpretation of the experimental data, and that of all the authors cited above, depends of course on the validity of the theory, linking q and ω to κ and σ for a body with the shape of a red cell in its native, hypotonic, and hypertonic states. The theory was developed for a planar membrane, and although it has given plausible results for large phospholipid vesicles (24), the geometry of the red cell in its physiological state departs considerably from this. Moreover, in its swollen, near-spherical state, the shape differs in important ways from the discoid form, where, for instance, two principal radii of curvature are required to define the rim. This question remains open.

ATP depletion

Our observations on ATP-depleted cells showed no discernible diminution of overall fluctuation amplitude or any change in its components. We have further replicated these results using the same experimental protocol and methods of analysis with two different imaging techniques, namely, phase-contrast and dark-field microscopy, and again found no measurable difference between intact and ATP-depleted cells. This appears to present a direct conflict with the work of Levin and Korenstein (17), and later articles from the same laboratory (18,19), which all record a large ATP-dependent component of the fluctuation, observed in dark-field. Apart from the difference in methodology, in that they measured fluctuations at a single point on the cell edge, the cells were apparently treated in the same manner as in our work. We have at present no explanation for the disparity between our results and theirs. Judged by our observations, at all events, the fluctuation appears to be thermal in character, as Parpart and Hoffman (3) originally concluded.

Physiological implications

Whether membrane fluctuations have any physiological role is unclear, but possible functions are readily envisaged, among them the control of adhesive phenomena, such as rouleau formation. Fluctuations may also govern, for instance, the propensity of swollen cells containing malaria parasites to attach to endothelial surfaces. Evidence, both theoretical and experimental, exists for a fluctuation-dependent repulsion between lipid bilayers (35). Local deformations of membrane curvature have been inferred to initiate the formation of coated vesicles from coated pits, through capture of the transient local invaginated state induced by undulations (36). Coated pits appear, though sparsely, in the red cell (37), but it is still unclear whether they participate in such receptor internalization events as occur in these cells. Calculations have also indicated (38) that undulatory movements of the membrane may control lateral diffusion of transmembrane proteins, in the red cell, notably, the anion exchanger, band 3, the cytoplasmic domain of which is thought to be entrapped in the interstices of the spectrin network (39,40). The clustering of receptors for endothelial surfaces and for soluble ligands is probably equally subject to such restraints. An additional function of membrane motions may be to facilitate diffusion in the cytosol of substrates and products of reaction, catalysed by membrane-associated glycolytic enzymes (41).

APPENDIX: EXTRACTION OF EDGE MOVEMENT FROM VIDEO RECORDINGS

This procedure is illustrated in Fig. 1. In short, each measurement comprised a 5-s video recording (125 frames). The approximate position of the cell edge was determined, using a thresholding method to give a pixel-wide strip around the cell periphery; 20–40 equally spaced points on this strip were then used to define a piecewise spline fit of the entire cell periphery as a ''reference profile'' for the precise measurement of the cell edge position. The spline-fit datum points gave the exact measurements around the cell in the orthogonal direction at equal angular intervals. Successive points were recorded at 1° angular intervals along the spline, and a square window, measuring 50×50 pixels, was extracted, centered on each point. The window was then rotated about its center, and a new pixel set was calculated (using cubic spline interpolation) to define a new x' axis of the pixel array, orthogonal to the cell edge. In this new position of the window, a narrow strip was extracted (5×50 pixels) and the pixel intensity across the y' direction of this strip summed to yield a plot of intensity against radial position. A consistent edge point could then be determined from the well-defined peak in the derivative of this signal. Its position could be located with subpixel precision, using a center-of-mass algorithm (42). This position was then transformed into the xy coordinate system with the centroid reference point of the cell as the origin. The edge positions around the cell for one video frame were then stored as a vector of

complex coordinates, combined in the form of a matrix, $E_{\theta,t}$, defining the periphery of the cell in space and time, such that the real and imaginary parts were, respectively, the x and y coordinates of the edge position at time t and angle θ.

It proved possible to make these measurements even on cells diffusing laterally on the agarose surface. This movement did not in general take the cells out of the field of view within the 5-s period of measurement, provided the magnification was chosen such that the width (and height) of the field was roughly twice the projected diameter. To analyze measurements on cells moving within this area, it was necessary to modify the measuring algorithm for the edge positions by recording the mean cell center position in each frame and moving the centroid position of the ''reference profile'' accordingly. It proved adequate to simply determine the reference profile from the first image and then translate it. Since most cell profiles are not precisely circular, this implied that the small translations were not accompanied by significant in-plane rotation.

Analysis of edge movement into its components

Having defined the mean centroid positions over the period of observation, C_t (Fig. 1); the distances from this to the points on the periphery were each averaged over all frames within the period of observation, and all were then averaged over all angles around the periphery to give the mean cell diameter $\overline{D}$ (Eq. A2); the complex matrix $E_{\theta,t}$ can then be reduced to the real matrix, $U_{\theta,t}$ (Eq. A3), which represents the absolute excursions of points on the cell from their mean positions:

$$C_t = \langle E_{\theta,t}\rangle_\theta; \tag{A1}$$

$$\overline{D} = 2\langle\langle|E_{\theta,t} - C_t|\rangle_t\rangle_\theta; \tag{A2}$$

$$U_{\theta,t} = |E_{\theta,t}| - \langle|E_{\theta,t}|\rangle_t. \tag{A3}$$

$U_{\vartheta,t}$ is then used to calculate the mean-square amplitude as a function of wave number and frequency, according to Eqs. 1 and 2 above, by the fast Fourier transform method. The space and time autocorrelation functions K_ϕ and K_τ can also be calculated and are, respectively,

$$K_\phi = \frac{\langle\langle U_{\theta,t}U_{\phi-\theta,t}\rangle_\theta\rangle}{\langle U^2\rangle}; \tag{A4}$$

$$K_\tau = \frac{\langle\langle U_{\theta,t}U_{\theta,\tau-t}\rangle_t\rangle_\theta}{\langle U^2\rangle}. \tag{A5}$$

Interpretation of the measured parameters

Out-of-plane fluctuations as a function of mode were derived for planar membranes by Helfrich and Servuss (8) on the basis of the equipartition theorem, as

$$\langle U(q_\perp)^2\rangle = \frac{k_BT}{\sigma q_\perp^2 + \kappa q_\perp^4}, \tag{A6}$$

where σ is the membrane tension and κ the bending modulus. Here we have measured only the radial membrane fluctuations at the cell periphery (i.e., q_x,, where $q_\perp^2 = q_x^2 + q_y^2$), and this projection, as solved by Pécréaux et al. (24,25), is given by Eq. 3 in the text. This can then be approximated for the limiting cases of $\sigma \gg \kappa$ and $\sigma \ll \kappa$, and by using Taylor's expansion reduces to Eqs. 4 and 5 (in the text). Although Eq. 3 refers in principle to a planar membrane, it has been demonstrated to be applicable to a spherical geometry for $q > 5$ (24). We have therefore made use of this equation, although we recognize that at the cell edge one of the principal radii is less than that of the discoid cell.

We thank Peter Petrov, Peter Winlove, and John Hale (University of Exeter), Pietro Cicuta and Young Zoon Yoon (University of Cambridge), J. F. Hoffman (Yale University), and our colleague Alex Lewalle for much valuable advice and discussion. We also thank the two anonymous reviewers for useful and perceptive comments.

REFERENCES

1. Mohandas, N., and E. Evans. 1994. Mechanical properties of the red cell membrane in relation to molecular structure and genetic defects. *Annu. Rev. Biophys. Biomol. Struct.* 23:787–818.
2. Browicz, T. 1890. Further observation of motion phenomena on red blood cells in pathological states. *Zbl. med. Wissen.* 28:625–627.
3. Parpart, A. K., and J. F. Hoffman. 1956. Flicker in erythrocytes; vibratory movements in the cytoplasm. *J. Cell. Physiol.* 47:295–303.
4. Brochard, F., and J. F. Lennon. 1975. Frequency spectrum of the flicker phenomenon in erythrocytes. *J. Phys.* 36:1035–1047.
5. Lennon, J. F. 1977. The flicker of the erythrocyte. PhD thesis. Université Paris-Sud,: Orsay, France.
6. Evans, E. A. 1983. Bending elastic modulus of red blood cell membrane derived from buckling instability in micropipet aspiration tests. *Biophys. J.* 43:27–30.
7. Scheffer, L., A. Bitler, E. Ben-Jacob, and R. Korenstein. 2001. Atomic force pulling: probing the local elasticity of the cell membrane. *Eur. Biophys. J.* 30:83–90.
8. Helfrich, W., and R. M. Servuss. 1984. Undulations, steric interaction and cohesion of fluid membranes. *Nuovo Cimento Soc. Ital. Fis.* 3D: 137–151.
9. Zilker, A., H. Engelhardt, and E. Sackmann. 1987. Dynamic reflection interference contrast (RIC-) microscopy: a new method to study surface excitations of cells and to measure membrane bending elastic-moduli. *J. Phys.* 48:2139–2151.
10. Strey, H., M. Peterson, and E. Sackmann. 1995. Measurement of erythrocyte membrane elasticity by flicker eigenmode decomposition. *Biophys. J.* 69:478–488.
11. Fricke, K., and E. Sackmann. 1984. Variation of frequency spectrum of the erythrocyte flickering caused by aging, osmolarity, temperature and pathological changes. *Biochim. Biophys. Acta.* 803:145–152.
12. Fricke, K., K. Wirthensohn, R. Laxhuber, and E. Sackmann. 1986. Flicker spectroscopy of erythrocytes. A sensitive method to study subtle changes of membrane bending stiffness. *Eur. Biophys. J.* 14: 67–81.
13. Zeman, K., H. Engelhardt, and E. Sackmann. 1990. Bending undulations and elasticity of the erythrocyte membrane: effects of cell shape and membrane organization. *Eur. Biophys. J.* 18:203–219.
14. Zilker, A., M. Ziegler, and E. Sackmann. 1992. Spectral-analysis of erythrocyte flickering in the 0.3–4-μ-M^{-1} regime by microinterferometry combined with fast image-processing. *Phys. Rev. A.* 46:7998–8002.
15. Peterson, M. A., H. Strey, and E. Sackmann. 1992. Theoretical and phase-contrast microscopic eigenmode analysis of erythrocyte flicker-amplitudes. *J. Phys. II.* 2:1273–1285.
16. Popescu, G., T. Ikeda, K. Goda, C. A. Best-Popescu, M. Laposata, S. Manley, R. R. Dasari, K. Badizadegan, and M. S. Feld. 2006. Optical measurement of cell membrane tension. *Phys. Rev. Lett.* 97:218101.
17. Levin, S., and R. Korenstein. 1991. Membrane fluctuations in erythrocytes are linked to MgATP-dependent dynamic assembly of the membrane skeleton. *Biophys. J.* 60:733–737.
18. Tuvia, S., S. Levin, A. Bitler, and R. Korenstein. 1998. Mechanical fluctuations of the membrane-skeleton are dependent on F-actin ATPase in human erythrocytes. *J. Cell Biol.* 141:1551–1561.
19. Tuvia, S., A. Almagor, A. Bitler, S. Levin, R. Korenstein, and S. Yedgar. 1997. Cell membrane fluctuations are regulated by medium macroviscosity: evidence for a metabolic driving force. *Proc. Natl. Acad. Sci. USA.* 94:5045–5049.
20. Lew, V. L., and H. G. Ferreira. 1978. Calcium transport and the properties of a calcium-activated potassium channel in red cell membranes. *Curr. Top. Membr. Trans.* 10:217–277.

21. Feo, C., and N. Mohandas. 1977. Clarification of role of ATP in red-cell morphology and function. *Nature*. 265:166–168.

22. Lew, V. L., and R. M. Bookchin. 1986. Volume, pH, and ion-content regulation in human red cells: analysis of transient behavior with an integrated model. *J. Membr. Biol*. 92:57–74.

23. Cokelet, G. R., and H. J. Meiselman. 1968. Rheological comparison of hemoglobin solutions and erythrocyte suspensions. *Science*. 162:275–277.

24. Pécréaux, J., H. G. Döbereiner, J. Prost, J. F. Joanny, and P. Bassereau. 2004. Refined contour analysis of giant unilamellar vesicles. *Eur. Phys. J. E. Soft Matter*. 13:277–290.

25. Pécréaux, J. 2004. Measurement of the fluctuation spectrum of giant vesicles by analysis of contours: application to passive and active membranes. PhD thesis. Université Pierre et Marie Curie, Paris.

26. Hategan, A., R. Law, S. Kahn, and D. E. Discher. 2003. Adhesively-tensed cell membranes: lysis kinetics and atomic force microscopy probing. *Biophys. J*. 85:2746–2759.

27. Eisinger, J., J. Flores, and R. M. Bookchin. 1984. The cytosol-membrane interface of normal and sickle erythrocytes. Effect of hemoglobin deoxygenation and sickling. *J. Biol. Chem.* 259:7169–7177.

28. Gov, N., A. G. Zilman, and S. Safran. 2003. Cytoskeleton confinement and tension of red blood cell membranes. *Phys. Rev. Lett*. 90:228101.

29. Rand, R. P., and A. C. Burton. 1964. Mechanical properties of the red cell membrane. I. Membrane stiffness and intracellular pressure. *Biophys. J*. 45:115–135.

30. Hochmuth, R. M. 1987. Properties of red blood cells. *In* Handbook of Bioengineering. R. Skalak and S. Chien, editors. McGraw-Hill, New York. 12.1–12.17.

31. Dai, J., M. P. Sheetz, X. Wan, and C. E. Morris. 1998. Membrane tension in swelling and shrinking molluscan neurons. *J. Neurosci*. 18:6681–6692.

32. Raucher, D., and M. P. Sheetz. 1999. Characteristics of a membrane reservoir buffering membrane tension. *Biophys. J*. 77:1992–2002.

33. Hochmuth, R. M., and W. D. Marcus. 2002. Membrane tethers formed from blood cells with available area and determination of their adhesion energy. *Biophys. J*. 82:2964–2969.

34. Hategan, A., K. Sengupta, S. Kahn, E. Sackmann, and D. E. Discher. 2004. Topographical pattern dynamics in passive adhesion of cell membranes. *Biophys. J*. 87:3547–3560.

35. Evans, E. A., and V. A. Parsegian. 1986. Thermal-mechanical fluctuations enhance repulsion between bimolecular layers. *Proc. Natl. Acad. Sci. USA*. 83:7132–7136.

36. Hinrichsen, L., A. Meyerholz, S. Groos, and E. J. Ungewickell. 2006. Bending a membrane: how clathrin affects budding. *Proc. Natl. Acad. Sci. USA*. 103:8715–8720.

37. Bar-Zvi, D., A. E. Levin, and D. Branton. 1987. Assembled clathrin in erythrocytes. *J. Biol. Chem*. 262:17719–17723.

38. Brown, F. L. 2003. Regulation of protein mobility via thermal membrane undulations. *Biophys. J*. 84:842–853.

39. Sheetz, M. P. 1983. Membrane skeletal dynamics: role in modulation of red cell deformability, mobility of transmembrane proteins, and shape. *Semin. Hematol*. 20:175–188.

40. Tomishige, M., Y. Sako, and A. Kusumi. 1998. Regulation mechanism of the lateral diffusion of band 3 in erythrocyte membranes by the membrane skeleton. *J. Cell Biol*. 142:989–1000.

41. Low, P. S., P. Rathinavelu, and M. L. Harrison. 1993. Regulation of glycolysis via reversible enzyme binding to the membrane protein, band 3. *J. Biol. Chem.* 268:14627–14631.

42. Patwardhan, A. 1997. Subpixel position measurement using 1D, 2D and 3D centroid algorithms with emphasis on applications in confocal microscopy. *J. Microsc*. 186:246–257.